SCIENTIFIC REPORTS

OPEN

SUBJECT AREAS:
SYNTHESIS OF GRAPHENE
ELECTRONIC DEVICES
ELECTRONIC MATERIALS
ELECTRONIC PROPERTIES AND MATERIALS

Received
5 November 2012

Accepted
4 January 2013

Published
7 February 2013

Correspondence and requests for materials should be addressed to Z.L. (zfliu@pku.edu.cn)

* These authors contributed equally to this work.

CVD Growth of Large Area Smooth-edged Graphene Nanomesh by Nanosphere Lithography

Min Wang[1]*, Lei Fu[1,2]*, Lin Gan[1], Chaohua Zhang[2], Mark Rümmeli[3], Alicja Bachmatiuk[3], Kai Huang[4], Ying Fang[4] & Zhongfan Liu[1]

[1]Center for Nanochemistry, Beijing National Laboratory for Molecular Sciences (BNLMS), State Key Laboratory for Structural Chemistry of Unstable and Stable Species, College of Chemistry and Molecular Engineering, Peking University, Beijing 100871, People's Republic of China, [2]Academy for Advanced Interdisciplinary Studies, Peking University, Beijing 100871, China, [3]IFW Dresden, PO Box 270116, D-01171 Dresden, Germany, [4]National Center for Nanoscience and Technology, 11 Beiyitiao Street, Zhongguancun, Beijing 100190, People's Republic of China.

Current etching routes to process large graphene sheets into nanoscale graphene so as to open up a bandgap tend to produce structures with rough and disordered edges. This leads to detrimental electron scattering and reduces carrier mobility. In this work, we present a novel yet simple direct-growth strategy to yield graphene nanomesh (GNM) on a patterned Cu foil via nanosphere lithography. Raman spectroscopy and TEM characterizations show that the as-grown GNM has significantly smoother edges than post-growth etched GNM. More importantly, the transistors based on as-grown GNM with neck widths of 65-75 nm have a near 3-fold higher mobility than those derived from etched GNM with the similar neck widths.

Graphene has attracted considerable interest in recent years as a result of its unique band structure and physical properties, including its extremely high carrier mobility, which makes graphene a promising candidate for future high-speed electronics and radio-frequency applications[1–4]. IBM researchers reported a 155 GHz graphene transistor, and even announced the first integrated circuit, fabricated from wafer-size graphene, demonstrating a broadband frequency mixer operating at frequencies up to 10 GHz[5]. However, it is still a major challenge to use graphene in CMOS based digital logic systems, since graphene is a gapless semiconductor and is not suitable for field-effect transistors operating at room temperature. Because quantum confinement effects can open a band gap, graphene nanostructures, such as graphene nanoribbons[6–10], graphene quantum dots[11] and graphene nanomesh (GNM)[12–15], have been fabricated for use in room-temperature switch transistors. Thus far, most efforts have employed post-synthesis etching strategies to process large graphene sheets into nanoscale graphene. This approach has been proven to be effective at opening a bandgap[6,9–14]. However, this method unavoidably produces rough and disordered edges due to the self-limitation of the etching process. Studies demonstrate that disordered edges on graphene nanostructures give rise to scattering of electrons and even reduce carrier mobility[16,17]. More seriously, the negative effect of disordered edges becomes much worse for graphene nanostructures with small sizes, which is critical for opening band gap of graphene. This is because its band gap is inversely proportional to its width and moreover it is highly sensitive to the type of edge termination[6]. Thus graphene nanostructures obtained by etching methods despite having a band gap tend to suffer from poor carrier mobilities. Recently, Sprinkle et al. reported the direct growth of graphene nanoribbon (GNR) with controlled widths of 40 nm on SiC substrates[18]. This represents a very different but effective approach without subsequent etching, which in principle enables the fabrication of graphene-nanoribbon transistors with both large band gap and high carrier mobility.

Growth of graphene on metal substrates is a more attractive approach because of its simplicity and the inherent ease with which the synthetic graphene can be transfered[19–22]. Very recently, Safron et al. reported the fabrication of GNR arrays and GNM via e-beam lithography and block copolymer lithography[23]. In this work, we show that large-scale graphene nanostructures can be directly grown on patterned copper (Cu) foil, which can be easily transferred for device application, and that the as-grown graphene nanostructures possess much smoother edges compared with etched counterpart, which is confirmed by direct observation with transmission electron microscopy (TEM). Herein, we take GNM as an example. Fig. 1 schematically illustrates our experimental design for the

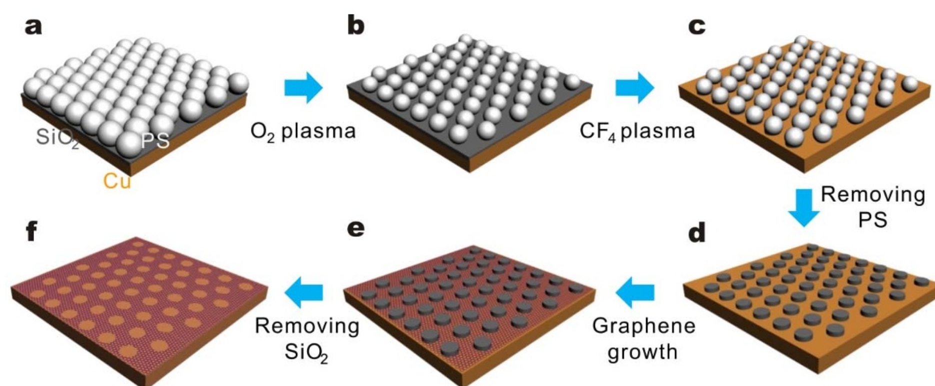

Figure 1 | Schematic illustration of our experimental design for direct growth of GNM on patterned Cu foil via nanosphere lithography. (a) A large-scale and close-packed monolayer of 230 nm PS nanosphere self-assembled onto SiO_2/Cu substrate. (b) Gaps forming between the close-packed PS nanospheres after O_2 plasma etching. (c) The exposed SiO_2 around each PS nanosphere removed by CF_4 plasma etching. (d) The periodic SiO_2 mask on Cu foil after removing PS nanospheres with toluene. (e) Graphene nucleation and growth on the exposed Cu surface around SiO_2 mask. (f) GNM obtained on Cu foil after removing periodic SiO_2 mask with HF acid.

direct growth of GNM on patterned Cu foil via nanosphere lithography. A SiO_2 film was first deposited on a Cu foil by an e-beam evaporator. This was followed by the formation of a large-scale and close-packed monolayer of polystyrene (PS) nanospheres through self-assembly over the SiO_2/Cu substrate (Fig. 1a). O_2 plasma etching was used to form gaps between the closely-packed PS nanospheres (Fig. 1b). A CF_4 plasma was then used to etch away the exposed SiO_2 around each PS nanosphere (Fig. 1c), and finally, a periodic SiO_2 mask could be obtained on the Cu foil after dissolving away the PS nanospheres with toluene (Fig. 1d). It should be noted that Copper fluoride probably forms on the Cu surface after SiO_2 etched by CF_4 plasma, which would lose fluorine and revert to Cu during high-temperature annealing process. The patterned Cu foil formed by the periodic SiO_2 mask was then used as a template for graphene growth using low-pressure chemical vapor deposition (CVD), which is a simple and commonly used approach for the production of large-scale graphene. Graphene nucleation and growth is only expected to proceed on the exposed Cu surface between the SiO_2 mask or discs (Fig. 1e). This approach enables one to obtain a GNM on Cu foil after removing the SiO_2 mask with HF acid (Fig. 1f). The employed experimental strategy is entirely based on low-cost, large-scale nanosphere lithography and provides a simple, yet efficient, way to grow ordered graphene nanostructures over a large area.

Results

Fig. 2a shows a scanning electron microscopy (SEM) image of the close-packed monolayer of PS nanospheres with a mean diameter of 230 nm. Gaps of around 40 nm form between the PS nanospheres after the air plasma etching process (Fig. 2b). Then the exposed SiO_2 film around the PS nanospheres was etched by a CF_4 plasma. Removal of the nanospheres by ultrasonic treatment in toluene followed. The SEM image in Fig. 2c confirms that a periodic SiO_2 mask on Cu foil can be obtained through the above-mentioned steps. It also shows that the width of the exposed copper tracks is slightly larger because the gap between each SiO_2 mask is several nm larger than that of the PS nanospheres because of the PS spherical morphology. After the graphene growth on the patterned Cu foil, the SiO_2 mask was removed and the graphene nano-mesh was then transferred onto SiO_2/Si substrates. The optical microscopy (OM) image in Fig. 2d shows a large-area and homogeneous single-layer GNM over SiO_2/Si. The low-magnification SEM image in Fig. 2e shows that the boundary lines exist in the as-grown GNM, and which correspond to the configuration defined by the PS nanosphere film (Supplementary Fig. S1d). The periodic black and gray color contrast presented in the high-magnification SEM image shown in Fig. 2f clearly demonstrates the GNM morphology. The atomic force microscopy (AFM) image presented in Fig. 2g further confirms a GNM structure, and shows a graphene thickness of ~1.1 nm except for some PMMA residues from the transfer process. This suggests that most of the as-grown GNM is single layer. Low voltage aberration-corrected, high-resolution TEM (LVAC-HRTEM) was employed to examine the microscopic structures of the obtained GNM. The HRTEM image in Fig. 2h and the corresponding Fourier transform (inset in Fig. 2h) highlights the single-crystal nature of the GNM neck. In Fig. 2i, a Fourier enhanced TEM micrograph of the marked area in Fig. 2h shows a single set of spots forming a hexagonal pattern which arises from graphene's 3-fold symmetry. Based on the above characterization results and analysis, we are able to draw the conclusion that large-area, high-quality and single-layer GNM can be directly grown on patterned Cu foil by periodic SiO_2 mask via nanosphere lithography.

Discussion

It is generally accepted that Cu catalytic action for graphene growth by low-pressure CVD method includes catalytic decomposition of a gaseous carbon source (CH_4) and subsequent nucleation and growth of graphene over the Cu surface[21]. Unlike metal catalysts such as Cu, SiO_2 has a significantly reduced catalytic activity with regards CH_4 decomposition, although two works show that molten SiO_2 nanoparticle (< 2 nm) can catalytically decompose the hydrocarbon molecules under certain circumstance[24,25]. Therefore, in general, graphene cannot easily nucleate and grow over the SiO_2 mask. In addition, we should be concerned whether there exists the possibility that graphene nucleates at the Cu-SiO_2 interface as this could affect the edge termination. After the high-temperature growth process, some periodic holes with 40 nm diameters and 10 nm depth were observed on the Cu foil by AFM after the 100 nm SiO_2 nanoparticles were removed with HF (Supplementary Fig. S2b). Van den Oetelaar et al. reported that nanometer-sized Cu particles were able to react with a SiO_2 substrate forming Cu silicide at 620°C under ultra-high vacuum[26]. So we believe that Cu_3Si, a typical Cu silicide, forms already at the Cu-SiO_2 interface before graphene growth, and that the evaporation of Cu_3Si with a melting point of 825°C results in the observed holes since growth occurs at 900°C. Therefore, it is unlikely that graphene can nucleate at the Cu-SiO_2 interface due to the presence of a high-energy barrier resulting from the strong interaction between Cu and SiO_2 during growth. Recently, however, Su et al. found that carbon pieces could diffuse through Cu grain boundaries and form graphene at a bulk Cu-SiO_2 interface[27]. In their work, the relatively weak interaction between the bulk Cu and SiO_2 substrate,

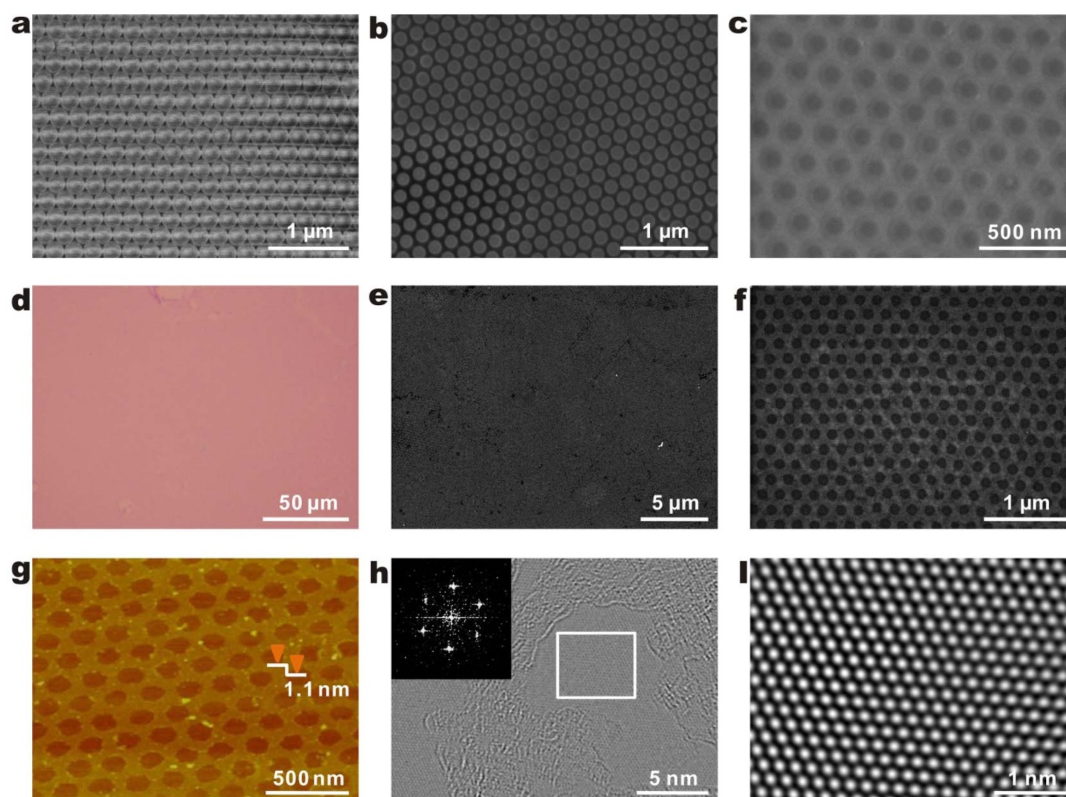

Figure 2 | Morphology and structure characterization of as-grown GNM. (a) SEM image of the close-packed monolayer of PS nanosphere with the diameter of 230 nm. (b) SEM image of PS nanosphere with ~40 nm gap after O_2 plasma etching. (c) SEM image of periodic SiO_2 mask on Cu foil after CF_4 plasma etching of the exposed SiO_2 and removing of PS nanosphere. (d) OM image of the large-area and homogeneous GNM on Si substrate with 300 nm SiO_2 after graphene growth on patterned Cu foil, removing of SiO_2 mask and the transfer of sample. (e) Low-magnification SEM image of the as-grown GNM showing the existence of boundary line resulted from the configuration of PS nanosphere film. (f) High-magnification SEM image of the GNM morphology. (g) AFM image of GNM structure with the thickness of ~1.1 nm except some PMMA residues from transfer process. (h) AC-HRTEM image and the corresponding Fourier transform of the single-crystal GNM neck. (i) Fourier enhanced TEM micrograph of the marked area in (h) showing a single set of a hexagonal spot pattern.

with lower activity than nanometer-sized counterparts, enables graphene nucleation at bulk Cu–SiO_2 interfaces. Our deduction is supported by their AFM and cross-sectional TEM images, in which no hole-like morphology forms at the bulk Cu–SiO_2 interface. Moreover, Safron et al. also reported similar graphene growth behavior on patterned Cu foil by Al_2O_3 mask, in which they found no graphene nucleation at Cu–Al_2O_3 interface[23]. For the CVD growth of graphene over poly-crystalline Cu it has been shown that graphene domains grow from different nucleation sites and then merge to form a large and continuous graphene layer[21,28,29], as shown in Supplementary Fig. S2e. Supplementary Figs. S2c and S2d show SEM images of graphene and GNM domains forming during the early growth stage. This observation suggests that a continuous GNM is also formed by the linkage of multiple GNM domains. Therefore, we speculate the following growth mechanism of the as-synthesized GNM. During growth, adsorbed CH_4 molecules decompose selectively on the exposed Cu surface to produce carbon atoms, the carbon atoms diffuse over the Cu surface, and then graphene nucleates at some preferential nucleation sites and grows. When graphene domains grow up to the Cu–SiO_2 boundary, the carbon supply depletes locally, thus inhibiting further growth which enables the GNM formation. Moreover, the GNM domains grow laterally and join on the continuous pattered Cu surface so as to form a large-area and contiguous GNM. The growth scheme of the GNM is illustrated in Supplementary Fig. S2f.

We also characterized the as-grown GNM by means of Raman spectroscopy. The Raman I_D/I_G ratio (where I_D and I_G are the D-band and G-band Raman intensities, respectively) is widely used to evaluate the graphene quality[30]. Fig. 3 shows the typical 632.8 nm laser excited Raman spectrum and statistics of I_D/I_G ratio for the as-grown GNM in the range of 0.6–0.9. I_D/I_G ratio of the as-grown GNM is smaller than most of reported values of GNM, GNR and other graphene nanostrucutures etched from exfoliated graphene[15,23,31–35], and is comparable to or a little larger than that of GNM and GNR obtained from direct growth, unzipping multiwalled carbon nanotubes, and nanoscale-cutting graphite method[10,23,35]. It should be noted that the as-grown GNM and the reported graphene nanostructures have different size. For rational comparison, an equivalent etched GNM sample (Supplementary Fig. S4) with similar neck width and periodic length (Supplementary Figs. S5e and S5f) was also characterized. Fig. 3 shows the typical Raman spectrum and statistics of I_D/I_G ratio for the post-growth etched GNM in the range of 1.1–1.7, which is comparable to the reported value of etched graphene nanostructures[15,23,31–35]. The average I_D/I_G ratio of as-grown GNM is almost two-fold smaller than that of the etched sample with similar neck width. The I_D/I_G ratio of GNM should be related to the density of defects in the nanomesh and its edge roughness[35,36]. Defects in a GNM can include point defects and line defects (viz. grain boundaries). The as-grown GNM and the as-produced graphene used as the source for the post-growth etched GNM, were grown under the exactly same CVD conditions, and thus point-defect differences between them can be ignored. From Supplementary Figs. S2c and S2d, we can see that the domain size of as-grown GNM is smaller than that of the graphene sample, which indicates that the line-defect density of as-grown GNM should be larger than that of the post-growth etched GNM. Therefore, the

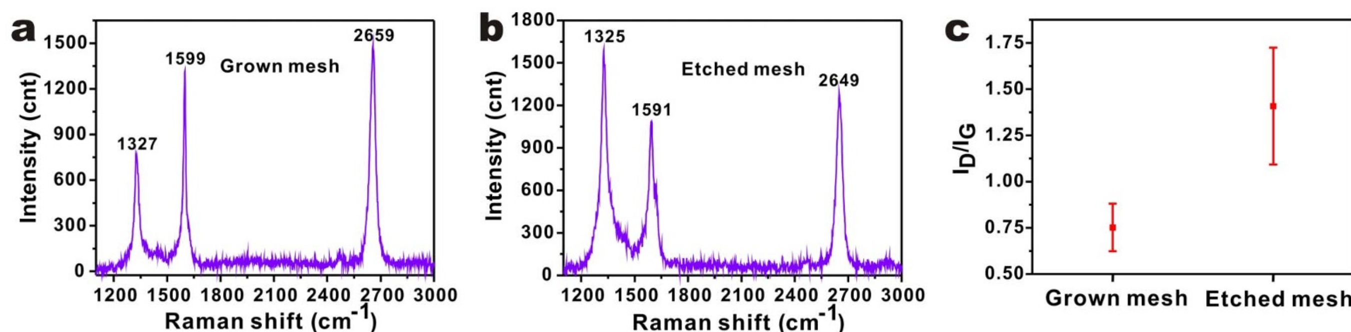

Figure 3 | Raman characterization of GNM after transfer. Typical Raman spectra of (a) as-grown and (b) post-growth etched GNM on SiO_2/Si substrate after transfer. (c) Statistics of I_D/I_G ratio for as-grown and post-growth etched GNM on SiO_2/Si substrate.

smaller I_D/I_G ratio (higher quality) of the as-grown GNM can be attributed to it having smoother graphene edges.

The edge roughness of both the GNM was characterized by HRTEM. The nanomesh structure is visible in the HRTEM images of the directly grown GNM (Fig. 4a) and of the post-growth etched GNM (Fig. 4d). The TEM images of edges from other as-grown GNM holes can be seen in Supplementary Figs. S3a–S3c. From the higher magnification HRTEM images in Figs. 4b and 4c and Supplementary Figs. S3a–S3c, we estimated the edge roughness of ~0.2 nm for the as-grown nanomesh, which is comparable to or even smoother than GNR obtained from nanoscale-cutting graphite method[10]. The observed maximum length of the smooth edge is up to ~30 nm, except the dent position (marked by white arrow in Supplementary Fig. S3b) due to the SiO_2 mask with rough edges caused by CF_4 plasma etching. We also found some ultra-smooth bi-layer edges shown in Supplementary Fig. S3c, which are similar to the graphite nanoribbon edges reconstructed by Joule heating inside a TEM-STM system[37]. Whereas the post-growth etched GNM edge is so rough, and even in the length range of ~40 nm we cannot see the smooth area, as shown in Figs. 4e and 4f. The roughness of post-growth etched GNM edge is about ~1 nm, which is similar to the value of the etched GNM edge reported by Safron et al.[15]. So the rough edge is a general issue for the etched GNM due to the self-limitations of plasma etching method. Our relatively massive observation of GNM edges at dozens of nm length from different holes directly and solidly shows that the as-grown GNM is much smoother than post-growth etched GNM. In the case of the post-growth etched GNM, the synthetic graphene copies the mask morphology, and its edge roughness should be larger than the mask edge roughness due to the self-limitation of plasma etching method. While for the as-grown GNM, after high-temperature annealing, the edge of the mask used for patterning Cu foil is probably smoother than that of the mask used in the post-growth etching route without annealing treatment, moreover, during the growth process the thermal energy causes the GNM edges to remain smooth as this reduces the system energy. Jia et al. demonstrated that disorder in edges of graphite nanoribbons could be shaped into zigzag or armchair edges by reconstruction process induced by Joule heating inside a TEM-STM system[37].

Transport measurements were performed to evaluate and compare the electronic properties of the as-grown and post-growth etched GNM with similar neck widths and periodic lengths (Supplementary Figs. S5e and S5f). Photolithography was used to fabricate field-effect transistors with channel lengths of $L = 2$ μm and widths of $W = 1$ μm, after the GNM had been transferred onto a Si substrate with a 300 nm SiO_2 surface layer. The device structure is illustrated in Fig. 5a. 5 nm Cr and 50 nm Au was used as the electrical contact metal for the source and drain electrodes. The doped Si substrate served as a global back gate to modulate the charge density in the graphene. To reduce the doping effect of H_2O and O_2 species adsorbed on graphene surface, the measurement was carried out in a vacuum chamber after current annealing[38]. Fig. 5b shows the typical transfer characteristics for devices based on the as-grown and post-growth etched GNM for a source-drain voltage $V_d = 10$ mV. The low on-off ratio of as-grown GNM transistor proves that a band gap is not present at room temperature. This is because the neck width (65–75 nm) of our GNM is larger than the critical size (~10 nm) for opening a band gap at room temperature[6,7]. The Dirac point of the as-grown and post-growth etched GNM graphene device is found at a

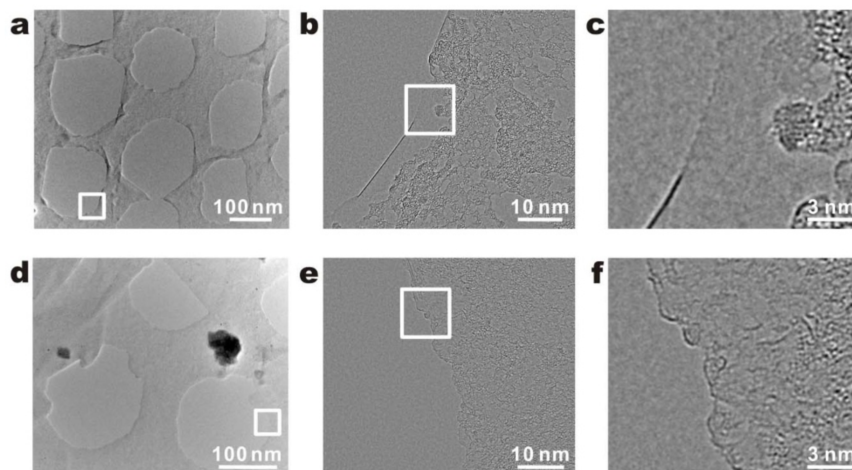

Figure 4 | Edge Characterization of GNM by TEM. TEM image of (a) as-grown (d) post-growth etched GMN. (b), (e) Enlarged TEM image of marked area in (a), (d), respectively. (c), (f) Enlarged TEM image of marked area in (b), (e), respectively.

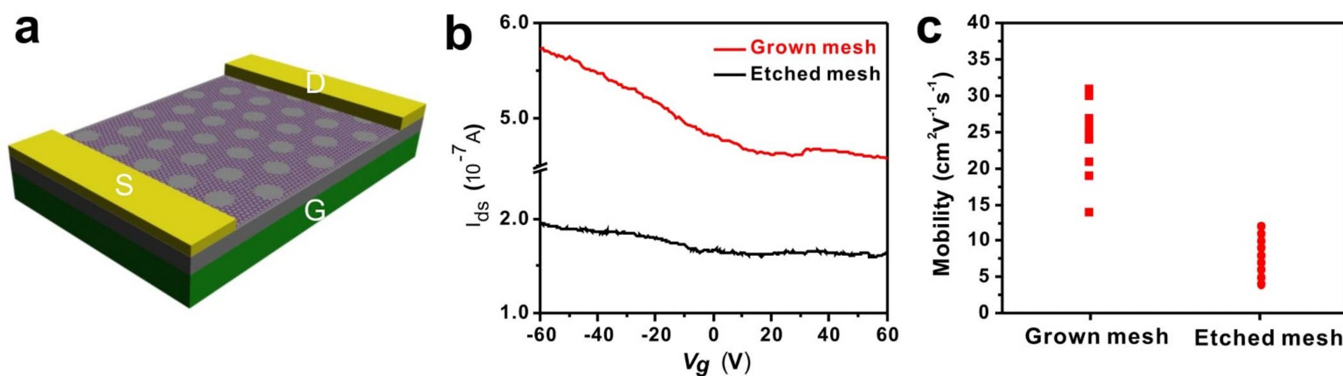

Figure 5 | Electrical measurement of GNM-based transistor. (a) Schematic illustration of GMN transistor structure with channel length of 2 μm and width of 1 μm. (b) Typical transfer characteristics for transistor devices based on as-grown and post-growth etched GNM at source-drain voltage V_d = 10 mV. (c) Statistics of the hole mobility of as-grown and post-growth etched GNM transistor devices.

gate voltage V_g = 25 and 15 V, respectively. The hole mobility was calculated using the equation

$$\mu = d\sigma/(C_g \cdot dV_g) = (L/C_g W V_d)\cdot(dI_d/dV_g)$$

where μ is the field effect mobility, C_g is the gate capacitance of the SiO_2 dielectric, and Id is the drain current. dI_d/dV_g was calculated from the slope between $V_g = -60$ V and V_g at the Dirac point. The calculated hole carrier mobility of the as-grown and post-growth etched GNM was 24 and 8 $cm^2 V^{-1} s^{-1}$, respectively. Fig. 5c shows a summary of the hole mobility for various devices for both GNM samples. Devices based on directly grown GNM have mobilities in the range of 13 to 31 $cm^2 V^{-1} s^{-1}$. Our CVD-graphene-nanomesh based transistor carrier mobility is about 1 order of magnitude lower than that of transistor based on unpatterned graphene[39,40]. Because of the relatively large neck width of as-grown GNM, the obtained hole mobility in our work is 1 order of magnitude larger than the value 1 $cm^2 V^{-1} s^{-1}$ of exfoliated-graphene-nanomesh with neck width of ~18 nm and 7–15 nm reported by Safron et al. and Kim et al., respectively, which is 3 order of magnitude smaller than the unpatterned exfoliated-graphene transistor mobility 1000–3000 $cm^2 V^{-1} s^{-1}$ [15,31]. In contrast, the mobility for post-growth etched GNM with similar neck widths and periodic lengths is in the range of 4 to 11 $cm^2 V^{-1} s^{-1}$, as shown in Fig. 5c. It means that the transistors based on as-grown GNM with neck widths of 65–75 nm have a near 3-fold higher mobility than those derived from post-growth etched GNM with the similar neck widths and periodic lengths. It has been shown that the carrier mobility of graphene-based transistors on SiO_2 substrate is limited by scattering from charged surface states and impurities, and SiO_2 surface optical phonons[41,42]. In our work, the external effect upon the device mobility for the as-grown and post-growth etched GNM should remain the same because the same SiO_2 substrate is used and, in addition, the same device fabrication process is employed. In case of nanostructured graphene such as nanomeshes and nanoribbons, disordered edges will produce serious scattering and compromise the carrier mobility as compared to large area graphene. Hence, the fact that the as-grown GNM transistor has higher mobility than post-growth etched GNM transistor again highlights the superior edge smoothens the GNM produced by our facile direct synthesis route.

In summary, we have successfully demonstrated a novel yet simple direct-growth strategy to yield CVD grown GNM with smooth edges over a large area on patterned Cu foil via nanosphere lithography. Raman and TEM characterizations show that the as-grown GNM has significantly smoother edges than post-growth etched GNM. More importantly, the transistor devices based on as-grown GNM possesses about 3-fold higher mobility. The developed templated growth method can be easily extended for the direct growth of other graphene nanostructures, such as graphene nanoribbons and quantum dots. Further efforts should be made to directly grow sufficiently small graphene nanostructures with band gaps at room temperature and high carrier mobility suitable for graphene electronics.

Methods

Assembly of PS monolayer on SiO_2/Cu substrate. 10% water dispersion containing monodisperse PS nanosphere with diameter of 230 nm was purchased from Unisize Technology (Changzhou) Co., LTD. 10 μL water/ethanol (volume ratio 1 : 1) dispersion was dropped onto the top surface of a 1 × 1 cm piece of Si substrate with 300 nm SiO_2, surrounded by water located at the midbottom of a glass dish, as shown in left part of Supplementary Fig. S1a. The dispersion spread freely on the water surface and generated a discontinuous monolayer film, as shown in middle part of Supplementary Fig. S1a. A drop of sodium dodecyl sulfate (SDS) solution could alter the surface tension and make a continuous monolayer film, as shown in right part of Supplementary Fig. S1a. Then the PS monolayer film was picked up with 25 μm thick Cu foil (Alfa Aesar, #13382) covered by 15 nm SiO_2 film using e-beam evaporator, which was treated by air plasma in advance for hydrophilic surface. After natural drying in air for half an hour, the assembly of PS monolayer on SiO_2/Cu substrate was succeeded.

Graphene and GNM growth. The Cu foil and patterned one by periodic SiO_2 mask were used as a substrate for graphene and GNM growth by low-pressure CVD method under the same condition. The furnace temperature rose from room temperature to 900°C in 25 min with H_2 flow rate of 10 sccm and pressure of 75 Pa, followed by a 10 min annealing process. Afterward, CH_4 with flow rate of 8 sccm was introduced for graphene growth, the pressure was increased to 125 Pa, and the duration is 10 min. After growth, the furnace cooled down to room temperature within 1 h.

Post-growth etched GNM. After growth of graphene on Cu foil under the same condition with GNM, graphene/Cu was used as the substrate for assembly of PS monolayer film, which is similar to the assembly of PS film on SiO_2/Cu substrate without plasma etching process. The alumina precursor was deposited in between the interstices of PS nanosphere from a DI-water: Triton-X-100 (400:1) solution of 0.25 M $Al(NO_3)_3$ via spin-coating at 8000 rpm. The substrate was annealed on a hot plate at 80°C for 15 min to oxidize the precursor into Al_2O_3, and then PS nanosphere was removed by immersion in toluene for 2 min, leaving behind Al_2O_3 mask on graphene/Cu, as shown in Supplementary Fig. S4a. After fabricating Al_2O_3 mask on graphene, the exposed graphene was etched away by air plasma (Femto, Diener Electronics) with the flow rate of 10 sccm, power of 90 w and time of 20 s.

GNM transfer. The as-grown and post-growth etched GNM sample were immersed in 2% HF for 1 h to remove SiO_2 or Al_2O_3 mask on Cu foil, and was then transferred onto silicon substrates with 300 nm thick SiO_2. Transfer of both as-grown and post-growth etched GNM onto SiO_2/Si substrate was conducted as our previous work[43]. 5% solution of 996K PMMA (Sigma Aldrich, #182265) in anisole was spin-coated onto GNM/Cu foil, and then the sample coated with PMMA was baked on a hot plate at 170°C for 5 min. Graphene on the back side of Cu foil was etched off by air plasma. 2.0 mol/L $FeCl_3$ acid solution was used for the etching of Cu foil. After cleaning by thin hydrochloric acid and DI water, GNM supported by PMMA film was picked up by SiO_2/Si substrate. PMMA was then removed by immersing in boiling acetone heated by hot plate with 170°C for 1 min. The obtained samples on SiO_2/Si substrate can be directly used for OM, SEM, Raman and TEM characterization and transistor fabrication. While before AFM measurement and TEM characterization, the samples were annealed in H_2/Ar at 350°C for 2 h to remove PMMA residuals.

Characterization. Optical images were taken with an optical microscope (Olympus DX51, Olympus), and Raman spectroscopy was performed with a laser micro-Raman spectrometer (Renishaw RM1000, Renishaw, 632.8 nm excitation wavelength). The scanning electron microscopy image was taken with a FEI-sFEG-XL30 microscope (FEI). The AFM images were taken with a Veeco Nanoscope IIIa (Veeco) after GNM transferred onto the 300-nm SiO_2/Si. The TEM images were taken with an aberration-corrected, high-resolution TEM (AC-HRTEM, JEOL 2010F) with GNM samples directly transferred onto a Cu grid. The current (I)–voltage (V) data were collected in the probe station under vacuum (4×10^{-3} torr).

1. Novoselov, K. S. *et al.* Electric field effect in atomically thin carbon films. *Science* **306**, 666–669 (2004).
2. Geim, A. K. & Novoselov, K. S. The rise of graphene. *Nat. Mater.* **6**, 183–191 (2007).
3. Orlita, M. *et al.* Approaching the Dirac Point in High-Mobility Multilayer Epitaxial Graphene. *Phys. Rev. Lett.* **101**, 267601 (2008).
4. Lin, Y. M. *et al.* 100-GHz Transistors from Wafer-Scale Epitaxial Graphene. *Science* **327**, 662–662 (2010).
5. Lin, Y. M. *et al.* Wafer-Scale Graphene Integrated Circuit. *Science* **332**, 1294–1297 (2011).
6. Han, M. Y., Ozyilmaz, B., Zhang, Y. B. & Kim, P. Energy band-gap engineering of graphene nanoribbons. *Phys. Rev. Lett.* **98**, 206805 (2007).
7. Li, X. L., Wang, X. R., Zhang, L., Lee, S. W. & Dai, H. J. Chemically derived, ultrasmooth graphene nanoribbon semiconductors. *Science* **319**, 1229–1232 (2008).
8. Kosynkin, D. V. *et al.* Longitudinal unzipping of carbon nanotubes to form graphene nanoribbons. *Nature* **458**, 872–U875 (2009).
9. Jiao, L. Y., Zhang, L., Wang, X. R., Diankov, G. & Dai, H. J. Narrow graphene nanoribbons from carbon nanotubes. *Nature* **458**, 877–880 (2009).
10. Mohanty, N. *et al.* Nanotomy-based production of transferable and dispersible graphene nanostructures of controlled shape and size. *Nat. Commun.* **3**, 844 (2012).
11. Ponomarenko, L. A. *et al.* Chaotic dirac billiard in graphene quantum dots. *Science* **320**, 356–358 (2008).
12. Bai, J. W., Zhong, X., Jiang, S., Huang, Y. & Duan, X. F. Graphene nanomesh. *Nat. Nanotechnol.* **5**, 190–194 (2010).
13. Liang, X. G. *et al.* Formation of Bandgap and Subbands in Graphene Nanomeshes with Sub-10 nm Ribbon Width Fabricated via Nanoimprint Lithography. *Nano Lett.* **10**, 2454–2460 (2010).
14. Sinitskii, A. & Tour, J. M. Patterning Graphene through the Self-Assembled Templates: Toward Periodic Two-Dimensional Graphene Nanostructures with Semiconductor Properties. *J. Am. Chem. Soc.* **132**, 14730–14732 (2010).
15. Safron, N. S., Brewer, A. S. & Arnold, M. S. Semiconducting Two-Dimensional Graphene Nanoconstriction Arrays. *Small* **7**, 492–498 (2011).
16. Tapaszto, L., Dobrik, G., Lambin, P. & Biro, L. P. Tailoring the atomic structure of graphene nanoribbons by scanning tunnelling microscope lithography. *Nat. Nanotechnol.* **3**, 397–401 (2008).
17. Wang, H. M., Wu, Y. H., Cong, C. X., Shang, J. Z. & Yu, T. Hysteresis of Electronic Transport in Graphene Transistors. *Acs Nano* **4**, 7221–7228 (2010).
18. Sprinkle, M. *et al.* Scalable templated growth of graphene nanoribbons on SiC. *Nat. Nanotechnol.* **5**, 727–731 (2010).
19. Yu, Q. K. *et al.* Graphene segregated on Ni surfaces and transferred to insulators. *Appl. Phys. Lett.* **93**, 113103 (2008).
20. Kim, K. S. *et al.* Large-scale pattern growth of graphene films for stretchable transparent electrodes. *Nature* **457**, 706–710 (2009).
21. Reina, A. *et al.* Large Area, Few-Layer Graphene Films on Arbitrary Substrates by Chemical Vapor Deposition. *Nano Lett.* **9**, 30–35 (2009).
22. Li, X. S. *et al.* Large-Area Synthesis of High-Quality and Uniform Graphene Films on Copper Foils. *Science* **324**, 1312–1314 (2009).
23. Safron, N. S., Kim, M., Gopalan, P. & Arnold, M. S. Barrier-Guided Growth of Micro- and Nano-Structured Graphene. *Adv. Mater.* **24**, 1041–1045 (2012).
24. Liu, B. L. *et al.* Metal-Catalyst-Free Growth of Single-Walled Carbon Nanotubes. *J. Am. Chem. Soc.* **131**, 2082–2083 (2009).
25. Huang, S. M., Cai, Q. R., Chen, J. Y., Qian, Y. & Zhang, L. J. Metal-Catalyst-Free Growth of Single-Walled Carbon Nanotubes on Substrates. *J. Am. Chem. Soc.* **131**, 2094–2095 (2009).
26. van den Oetelaar, L. C. A., van den Oetelaar, R. J. A., Partridge, A., Flipse, C. F. J. & Brongersma, H. H. Reaction of nanometer-sized Cu particles with a SiO_2 substrate. *Appl. Phys. Lett.* **74**, 2954–2956 (1999).
27. Su, C. Y. *et al.* Direct Formation of Wafer Scale Graphene Thin Layers on Insulating Substrates by Chemical Vapor Deposition. *Nano Lett.* **11**, 3612–3616 (2011).
28. Li, X. S., Cai, W. W., Colombo, L. & Ruoff, R. S. Evolution of Graphene Growth on Ni and Cu by Carbon Isotope Labeling. *Nano Lett.* **9**, 4268–4272 (2009).
29. Li, X. S. *et al.* Graphene Films with Large Domain Size by a Two-Step Chemical Vapor Deposition Process. *Nano Lett.* **10**, 4328–4334 (2010).
30. Ni, Z. H., Wang, Y. Y., Yu, T. & Shen, Z. X. Raman Spectroscopy and Imaging of Graphene. *Nano Res.* **1**, 273–291 (2008).
31. Kim, M., Safron, N. S., Han, E., Arnold, M. S. & Gopalan, P. Fabrication and Characterization of Large-Area, Semiconducting Nanoperforated Graphene Materials. *Nano Lett.* **10**, 1125–1131 (2010).
32. Liu, L. *et al.* Nanosphere Lithography for the Fabrication of Ultranarrow Graphene Nanoribbons and On- Chip Bandgap Tuning of Graphene. *Adv. Mater.* **23**, 1246–1251 (2011).
33. Begliarbekov, M. *et al.* Localized States and Resultant Band Bending in Graphene Antidot Superlattices. *Nano Lett.* **11**, 1254–1258 (2011).
34. Akhavan, O. Graphene Nanomesh by ZnO Nanorod Photocatalysts. *Acs Nano* **4**, 4174–4180 (2010).
35. Jiao, L. Y., Wang, X. R., Diankov, G., Wang, H. L. & Dai, H. J. Facile synthesis of high-quality graphene nanoribbons. *Nat. Nanotechnol.* **5**, 321–325 (2010).
36. Gupta, A. K., Russin, T. J., Gutierrez, H. R. & Eklund, P. C. Probing Graphene Edges via Raman Scattering. *Acs Nano* **3**, 45–52 (2009).
37. Jia, X. T. *et al.* Controlled Formation of Sharp Zigzag and Armchair Edges in Graphitic Nanoribbons. *Science* **323**, 1701–1705 (2009).
38. Moser, J., Barreiro, A. & Bachtold, A. Current-induced cleaning of graphene. *Appl. Phys. Lett.* **91**, 113103 (2007).
39. Yan, K., Peng, H. L., Zhou, Y., Li, H. & Liu, Z. F. Formation of Bilayer Bernal Graphene: Layer-by-Layer Epitaxy via Chemical Vapor Deposition. *Nano Lett.* **11**, 1106–1110 (2011).
40. Dai, B. Y. *et al.* Rational design of a binary metal alloy for chemical vapour deposition growth of uniform single-layer graphene. *Nat. Commun.* **2**, 522 (2011).
41. Ando, T. Screening effect and impurity scattering in monolayer graphene. *J. Phys. Soc. Jpn.* **75**, 074716 (2006).
42. Chen, J. H., Jang, C., Xiao, S. D., Ishigami, M. & Fuhrer, M. S. Intrinsic and extrinsic performance limits of graphene devices on SiO_2. *Nat. Nanotechnol.* **3**, 206–209 (2008).
43. Reina, A. *et al.* Transferring and Identification of Single- and Few-Layer Graphene on Arbitrary Substrates. *J. Phys. Chem. C* **112**, 17741–17744 (2008).

Acknowledgments

The research was supported by the Natural Science Foundation of China (Grants 51072004, 50821061, 50802003, 20973013, 20833001) and the Ministry of Science and Technology of China (Grants 2007CB936203, 2009CB29403). AB thanks the Alexander von Humboldt Foundation and the BMBF. MHR thanks the EU and the Freistat Sachsen.

Author contributions

M. W., L. F., L. G. C. Z. and K. H. performed the experiments. M. W., L. F. and Z. L. designed research and wrote the manuscript. All authors discussed the results and commented on the manuscript.

Additional information

Supplementary information accompanies this paper at http://www.nature.com/scientificreports

Competing financial interests: The authors declare no competing financial interests.

License: This work is licensed under a Creative Commons Attribution-NonCommercial-NoDerivativs 3.0 Unported License. To view a copy of this license, visit http://creativecommons.org/licenses/by-nc-nd/3.0/

How to cite this article: Wang, M. *et al.* CVD Growth of Large Area Smooth-edged Graphene Nanomesh by Nanosphere Lithography. *Sci. Rep.* **3**, 1238; DOI:10.1038/srep01238 (2013).